

Majorana Fermions in spin up and down electronic complexes in spin-orbit coupled array of semiconductor quantum dots in proximity to *s*-type superconductor and in magnetic field

Mijanur Islam,^{1,*} Mahan Mohseni,¹ Ibsal Assi,^{1,†} Daniel Miravet,¹ and Paweł Hawrylak¹

¹*Department of Physics, University of Ottawa, Ottawa, Ontario, K1N 6N5, Canada.*

(Dated: January 22, 2026)

Semiconductor–*s*-type superconductor nanowires host spinful fermions and cannot be reduced to a single spinless Kitaev chain hosting single Majorana zero mode. Instead, such systems can be converted into two coupled *p*-wave Kitaev-like chains associated with different spin sectors. Using the bond Fermion transformation and exact diagonalization, we analyze parity resolved spectra and local spectral functions, demonstrating that zero-energy modes strongly localized at the system boundaries emerge only in one effective chain. Inter-chain coupling lifts parity degeneracy and redistributes the low-energy spectral weight, providing a controlled framework to assess the stability of Majorana-like modes in the finite spinful nanowires.

I. INTRODUCTION

Topological superconductors hosting Majorana zero modes (MZMs) have attracted intense interest as a promising platform for fault tolerant quantum computation, where information is stored non-locally and manipulated through non-Abelian braiding operations [1–5]. A minimal model for an array of semiconductor (SM) quantum dots hosting one type of spin Fermions with nearest neighbor tunneling and *p*-type superconducting pairing due to proximity with a *p*-type superconductor (SC), which supports zero energy Majorana bound states localized at the ends of the chain in its topological phase is the Kitaev chain [1]. Braiding of MZM is insensitive to the details of external potential and leads to MZM with long coherence times [5–7]. In realistic solid state devices based on *s*-type SC there are spin up and down electrons [8–10]. A key challenge is therefore to engineer an effective *p*-wave Kitaev Hamiltonian in which spin up–spin down electronic system with Rashba spin orbit coupling (SOC), Zeeman splitting and *s*-wave SC pairing maps onto two Kitaev like chains supporting different spin MZMs [2, 4, 11, 12]. The presence of two coupled MZMs affects potential braiding operation and is the subject of our study and many other works.

Semiconductor–superconductor (SM-SC) nanowires have emerged as the leading platform for realizing such an effective *s*-wave Hamiltonian [4, 11–13]. In the experimental setup, a one-dimensional InSb, InAs or WSe₂ nanowire with strong Rashba SOC is proximity coupled to potentially an *s*-wave superconductor and subjected to a magnetic field [11, 12, 14–16]. The combination of spin-orbit induced helical bands, Zeeman splitting and induced pairing potentially removes one spin species at low energy and produces a spinless *p*-wave like superconducting phase, isomorphic to the Kitaev chain [11, 12].

Despite substantial effort, a fully unambiguous demonstration

of topological Majorana physics in nanowires remains elusive. It is now well established that disorder, smooth confinement and quantum dot formation can generate Andreev bound states that mimic many spectroscopic signatures of MZMs, including robust zero-bias conductance peaks and apparent quantization of the conductance [17–19]. These observations have motivated increasingly sophisticated experimental designs and analysis protocols, as well as detailed theoretical modeling of realistic devices beyond the idealized single band nanowire [4, 17–19]. In this context, bottom up approaches that assemble an effective Kitaev chain from well controlled building blocks offer an appealing route to realizing and diagnosing the *s*-wave Hamiltonian at the few site level.

A particularly powerful strategy is to use chains of quantum dots (QDs) coupled via short superconducting segments [20–25]. In these devices, gate voltages can independently tune the dot energies, tunnel couplings, and induced pairing amplitudes, allowing direct control over the effective Kitaev parameters site by site [4, 26]. Early experiments on double QD “Andreev molecules” embedded in hybrid nanowires demonstrated strong, tunable hybridization between dot states mediated by elastic co-tunnelling, and crossed Andreev reflection, [20, 21] paving the way for the realization of a minimal two-site Kitaev chain. Such a minimal chain was subsequently implemented in coupled InSb QDs proximitized by an *s*-wave superconductor, where appropriate tuning led to so-called “poor man’s Majoranas” near zero-energy states localized at the ends of the two-site system [22, 27]. More recently, multi-dot chains with three or more sites have been used to enhance the topological gap and Majorana localization, demonstrating that extending the chain length substantially improves the robustness of the zero-energy modes [23–25, 28]. Machine-learning assisted tuning protocols have further enabled automated navigation of the high dimensional gate space to reliably reach the “sweet spots” of artificial Kitaev chains in experiment [29, 30].

In parallel with these developments, there has been substantial progress in the epitaxial growth and atomistic characterization of semiconductor nanowires containing arrays of embedded QDs. In particular, InAsP/InP nanowire QDs grown along the wurtzite *c*-axis provide clean confinement, large spin-orbit

* drmijanphysics25@gmail.com

† Present address: Department of Physics and Physical Oceanography, Memorial University of Newfoundland and Labrador, St. John’s, Newfoundland & Labrador, Canada A1B 3X7

coupling and excellent optical and electronic properties, making them an attractive platform for implementing QD-based Kitaev chains [31–35]. Detailed atomistic tight-binding studies have established that the electronic structure, Coulomb interactions, and tunnel couplings in such nanowire QD arrays can be engineered with high precision by controlling the dot composition, geometry and axial spacing [31, 32, 36]. Building on this materials platform, recent theoretical work has shown that a chain of InAsP QDs embedded in an InP nanowire and proximitized by an *p*-wave superconductor can realize a Kitaev chain supporting non-local MZMs and even bound electron–hole excitations [37]. Moreover, recent advances in the theoretical and experimental understanding of the optical emission and absorption spectra of nanowire embedded quantum dots indicate that these systems provide experimentally viable routes for the realization and spectroscopic detection of Majorana bound states in semiconductor quantum dot based nanowire devices [38–40].

These advances naturally motivate a search for microscopic description of the *s*-wave Hamiltonian that is tailored to spinful QD chains in realistic nanowire devices. In such structures, electrons tunneling between dots experience strong Rashba SOC due to structural inversion asymmetry, while an external magnetic field generates a Zeeman splitting field that is orthogonal to the spin-orbit field. Proximity to an *s*-wave superconductor induces an on-site pairing amplitude, resulting in a spinful tight-binding Hamiltonian with hopping, SOC, Zeeman and pairing terms [13, 41]. At low energies and in appropriate parameter regimes, this spinful model can be mapped onto Kitaev chain associated with different spin or band projections, effectively realizing a *p*-wave generalization of the Kitaev Hamiltonian that is directly relevant to current experiments on hybrid nanowires and QD arrays [4, 11, 12]. Considerable effort has been devoted to establishing a connection between the Kitaev chain and realistic Majorana nanowires [41, 42]. However, a detailed understanding of how the underlying spinful *s*-wave Hamiltonian encodes topological phases, fermion-parity sectors, and low-lying excitations remains essential for interpreting experimental spectra and for the design of robust Majorana devices.

In this work we develop and analyze the spinful *s*-wave Hamiltonian appropriate for a chain of semiconductor QDs with Rashba SOC and Zeeman splitting, embedded in an InP nanowire and proximitized by an *s*-wave superconductor. We combine exact diagonalization (ED) in the full fermionic Fock space with a representation in terms of Majorana and bond Fermions to reveal the structure of the low-energy spectrum, the emergence of topological parity degeneracies and their lifting by inter-spin sector couplings. The resulting framework directly connects microscopic device parameters, such as hopping amplitudes, SOC strength, Zeeman field, pairing, and inter QD coupling to experimentally accessible observables such as parity splitting and local addition spectral functions measured in tunnelling spectroscopy. Our goal is to develop a quantitatively controlled and experimentally grounded description of the SM-SC Hamiltonian in realistic spinful nanowire hosting array of quantum-dots. In our

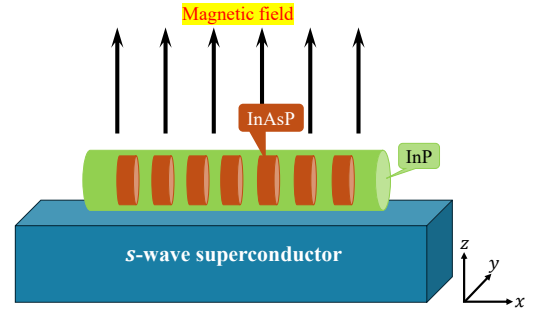


FIG. 1. Schematic illustration of an InP nanowire hosting an array of embedded InAsP quantum dots, proximity coupled to an *s*-wave superconductor and subjected to a perpendicular magnetic field, chosen to be orthogonal to the effective Rashba spin orbit coupling and thereby inducing Zeeman splitting.

framework, we introduce a fermionic transformation that reorganizes the spinful degrees of freedom, allowing the *s*-wave SM-SC Hamiltonian to be expressed as two effective *p*-wave Kitaev Hamiltonians associated with opposite spins, coupled by residual inter spin terms.

The structure of the paper is as follows. Section II introduces the model Hamiltonian of the system. In Section III, we present the exact diagonalization method, together with the relevant fermionic transformations, and introduce the Majorana and bond-fermion representations of the SM-SC Hamiltonian. The results are presented in Section IV. Finally, Section V summarizes our main findings.

II. MODEL HAMILTONIAN

As discussed earlier, we consider a hexagonal InP nanowire containing an array of embedded InAsP quantum dots [43–46] as shown in Fig. 1. Electrons confined to the wire experience Rashba SOC of strength α , and a Zeeman splitting V_z produced by an externally applied magnetic field (e.g. perpendicular to the spin quantization axis induced by Rashba SOC) so that it opens an energy gap. Proximity to an *s*-wave superconductor induces a pairing amplitude Δ in the wire [13]. The quantum dot array can be represented either as a periodic potential modulation (a superlattice) in a continuum Bogoliubov–de Gennes (BdG) model, or, in the limit of well isolated dots, as a tight binding chain of localized orbitals coupled by tunnel amplitudes. Such arrays have been widely investigated [31–34]. The current advanced fabrication techniques allow for controlling various aspects of this design. In the tight-binding approximation, the Hamiltonian for this system can be written as [13]

$$H_e = H_{TB} + H_\mu + H_{SOC} + H_z + H_\Delta, \quad (1)$$

where

$$H_{\text{TB}} = t \sum_{j=1, \sigma=\uparrow, \downarrow}^{N-1} (c_{j+1\sigma}^\dagger c_{j\sigma} + h.c.), \quad (2)$$

$$H_\mu = -\mu \sum_{j=1, \sigma=\uparrow, \downarrow}^N c_{j\sigma}^\dagger c_{j\sigma}, \quad (3)$$

$$H_{\text{SOC}} = \alpha \sum_{j=1}^{N-1} (c_{j+1\uparrow}^\dagger c_{j\downarrow} - c_{j+1\downarrow}^\dagger c_{j\uparrow} + h.c.), \quad (4)$$

$$H_z = V_z \sum_{j=1}^N (c_{j\uparrow}^\dagger c_{j\uparrow} - c_{j\downarrow}^\dagger c_{j\downarrow}), \quad (5)$$

$$H_\Delta = \Delta \sum_{j=1}^N (c_{j\downarrow}^\dagger c_{j\uparrow}^\dagger + h.c.). \quad (6)$$

Here $c_{i\sigma}^\dagger$ creates an electron in the dot i with spin σ , t is the nearest neighbor hopping (inter dot tunneling), μ is the on-site chemical potential. The SOC term is written in a gauge where the spin dependent hopping is proportional to σ_y and the Zeeman term is local and chosen along σ_z .

III. EXACT DIAGONALIZATION AND FERMIONIC REPRESENTATIONS

The Hamiltonian in Eq. (1) supports two MZMs localized at the ends of the chain when the system is in the topological regime [11–13]. After outlining the ED approach formulated in terms of normal fermions, we demonstrate how rewriting the problem in a Majorana basis naturally motivates the introduction of a new set of operators that we refer to as bond Fermions. This representation provides a particularly transparent way of organizing the Hilbert space and simplifies several aspects of the ED procedure.

A. Exact diagonalization in normal Fermion basis

We begin by introducing the ED method used to obtain the energy spectrum of the s-wave Hamiltonian. In ED, the Hilbert space is constructed in a configuration (occupation-number) basis. For an electronic system consisting of N spinful orbitals, the total Fock space dimension is 2^{2N} , since each orbital can be either empty or occupied for each spin projection. The basis states can therefore be written as

$$|n_{1\downarrow} \dots n_{N\downarrow}\rangle \otimes |n_{1\uparrow} \dots n_{N\uparrow}\rangle = \prod_{j=1}^N (c_{j\downarrow}^\dagger)^{n_{j\downarrow}} |0_\downarrow\rangle \otimes \prod_{j=1}^N (c_{j\uparrow}^\dagger)^{n_{j\uparrow}} |0_\uparrow\rangle, \quad (7)$$

where $|0\rangle$'s denote the electron vacuum in corresponding subspaces. Here $n_{j\sigma} \in \{0, 1\}$ specifies whether the orbital j with spin σ is unoccupied (0) or occupied (1). Each basis state is therefore generated by acting with creation operators on the vacuum according to its specified occupation numbers.

For a fixed electron number M , one can restrict Eq. (7) to only those configurations whose occupations satisfy

$$\sum_{j,\sigma} n_{j\sigma} = M. \quad (8)$$

The set of all such configurations is denoted by $\{|M, p_M\rangle\}$, where p_M labels different occupation patterns with the same total particle number M . However, the key physical point is that the s-wave Hamiltonian does not conserve particle number due to pairing terms. Individual basis states $|M, p_M\rangle$ are not eigenstates. As a result, the eigenstates must be superpositions of different particle-number sectors, i.e.,

$$|\psi^\nu\rangle = \sum_{M, p_M} C_{M, p_M}^\nu |M, p_M\rangle \quad (9)$$

where p_M enumerates all configurations with M electrons distributed among the $2N$ spin orbitals. To determine the coefficients C_{M, p_M}^ν , we apply the Hamiltonian to this state and use the orthogonality of the configuration basis to obtain the eigenvalue equation

$$\sum_{p_M, M} \langle q_{M'}, M' | H_e | p_M, M \rangle C_{M, p_M}^\nu = E^\nu C_{M', q_{M'}}^\nu. \quad (10)$$

Because the s-wave Hamiltonian, H_e , in Eq. (1) changes particle number only in pairs ($\Delta M = \pm 2$), the matrix element $\langle q_{M'}, M' | H_e | p_M, M \rangle$ is non-zero only when M and M' have the same fermion parity that is, both even or both odd. This symmetry allows the Hilbert space to be decomposed into two independent sectors corresponding to even and odd fermion parity.

B. Diagonalization of the Onsite Terms and the local BdG Transformation

We now locally diagonalize the on-site Hamiltonian by introducing a new set of fermionic quasiparticles. This procedure parallels the Bogoliubov transformation but is performed locally in real space. The resulting quasiparticles provide a physically transparent basis in which the on-site Hamiltonian is diagonal, and the remaining hopping and SOC terms acquire renormalized amplitudes and induced nonlocal pairing terms. This transformation is the first step toward constructing an effective low-energy description and enables a clean separation between single site physics and inter spin coupling.

I. Onsite Hamiltonian and its matrix form

We begin by isolating the on-site terms of the electronic Hamiltonian (Eq. (1)), containing the Zeeman field (Eq. (5)), chemical potential (Eq. (3)), and s-wave pairing (Eq. (6)):

$$H_{\text{onsite}} = \sum_{j=1}^N \left[(V_z - \mu) c_{j\uparrow}^\dagger c_{j\uparrow} - (V_z + \mu) c_{j\downarrow}^\dagger c_{j\downarrow} + \Delta (c_{j\downarrow}^\dagger c_{j\uparrow}^\dagger + c_{j\uparrow} c_{j\downarrow}) \right]. \quad (11)$$

It is convenient to rewrite Eq. (11) in the Nambu spinor basis $(c_{j\uparrow}, c_{j\downarrow}^\dagger)^T$ as

$$H_{\text{onsite}} = \sum_{j=1}^N \begin{pmatrix} c_{j\uparrow}^\dagger & c_{j\downarrow} \end{pmatrix} [A] \begin{pmatrix} c_{j\uparrow} \\ c_{j\downarrow}^\dagger \end{pmatrix} - N(V_z + \mu), \quad (12)$$

where the on-site BdG matrix is

$$A = V_z I - \mu \sigma_z - \Delta \sigma_x. \quad (13)$$

This 2×2 Hermitian matrix has the eigenvalues

$$\lambda_{\pm} = V_z \pm \sqrt{\mu^2 + \Delta^2}, \quad (14)$$

with normalized eigenvectors

$$\chi_1 = \begin{pmatrix} -\xi \\ 1 \end{pmatrix}, \quad \chi_2 = \begin{pmatrix} 1 \\ \xi \end{pmatrix}, \quad (15)$$

where

$$\xi = \frac{\Delta}{\mu + \sqrt{\mu^2 + \Delta^2}}, \quad = \frac{1}{\sqrt{1 + \xi^2}}. \quad (16)$$

The matrix A mixes particle and hole operators (via Δ). To simplify the structure of the Hamiltonian, it is advantageous to work in a basis that diagonalizes the on-site BdG matrix. We therefore define new fermionic operators $d_{j\sigma}$ by expanding the original Fermions in the eigenvectors of A as

$$\begin{pmatrix} c_{j\uparrow} \\ c_{j\downarrow}^\dagger \end{pmatrix} = \chi_1 d_{j\uparrow} + \chi_2 d_{j\downarrow}^\dagger = \begin{pmatrix} -\xi d_{j\uparrow} + d_{j\downarrow}^\dagger \\ d_{j\uparrow} + \xi d_{j\downarrow}^\dagger \end{pmatrix}. \quad (17)$$

The d -operators satisfy the canonical fermionic anticommutation relations $\{d_{i\sigma}, d_{j\sigma'}^\dagger\} = \delta_{ij} \delta_{\sigma\sigma'}$. Substituting the transformation (Eq. (17)) into Eq. (11) gives

$$H_{\text{onsite}} = \sum_{j=1}^N \left[\lambda_+ d_{j\uparrow}^\dagger d_{j\uparrow} - \lambda_- d_{j\downarrow}^\dagger d_{j\downarrow} \right] - N \left(\mu + \sqrt{\mu^2 + \Delta^2} \right), \quad (18)$$

which is fully diagonal in the new d -Fermion basis. Thus, the d -Fermions correspond to local quasiparticle operators obtained by diagonalizing the superconducting on-site physics.

2. Transformation of hopping and SOC terms

The remaining terms of the Hamiltonian (1), nearest neighbor hopping (Eq. (2)) and Rashba SOC term (Eq. (4)) must be rewritten in terms of the d operators. The hopping term (Eq. (2)) transforms as

$$\begin{aligned} H_{\text{TB}} = & \tilde{t} \sum_{j=1}^{N-1} [d_{j+1\uparrow}^\dagger d_{j\uparrow} + d_{j+1\downarrow}^\dagger d_{j\downarrow} + h.c.] \\ & + \Delta_t \sum_{j=1}^{N-1} [d_{j+1\uparrow}^\dagger d_{j\downarrow}^\dagger - d_{j+1\downarrow}^\dagger d_{j\uparrow}^\dagger + h.c.] \end{aligned} \quad (19)$$

with coefficients

$$\tilde{t} = -\frac{2t\mu^2\xi}{\Delta}, \quad \Delta_t = -2t^2\xi. \quad (20)$$

Thus, the hopping term results in a new renormalized hopping plus a superconducting like pairing between different lattice sites in terms of the new d operators. Similarly, the Rashba SOC term (Eq. (4)) transforms as

$$\begin{aligned} H_{\text{SOC}} = & \tilde{\alpha} \sum_{j=1}^{N-1} [d_{j+1\uparrow}^\dagger d_{j\downarrow} - d_{j+1\downarrow}^\dagger d_{j\uparrow} + h.c.] \\ & + \Delta_\alpha \sum_{j=1}^{N-1} [d_{j+1\uparrow}^\dagger d_{j\uparrow}^\dagger + d_{j+1\downarrow}^\dagger d_{j\downarrow}^\dagger + h.c.] \end{aligned} \quad (21)$$

with

$$\tilde{\alpha} = \frac{2\alpha\mu^2\xi}{\Delta}, \quad \Delta_\alpha = -2\alpha^2\xi. \quad (22)$$

Therefore, here also we ended up with a renormalized spin-orbit coupling plus a p -wave like pairing term.

3. Effective Hamiltonian in the d Fermion basis

Collecting all contributions, in the new operator basis the full electronic Hamiltonian Eq. (1) can be written as

$$H_e = H_\downarrow + H_\uparrow + H_{\downarrow\uparrow} - N \left(\mu + \sqrt{\mu^2 + \Delta^2} \right), \quad (23)$$

where the three components are

$$\begin{aligned} H_\sigma = & \tilde{t} \sum_{j=1}^{N-1} [d_{j+1\sigma}^\dagger d_{j\sigma} + h.c.] + \Delta_\alpha \sum_{j=1}^{N-1} [d_{j+1\sigma}^\dagger d_{j\sigma}^\dagger + h.c.] \\ & \pm \lambda_\pm \sum_{j=1}^N d_{j\sigma}^\dagger d_{j\sigma} \end{aligned} \quad (24a)$$

$$\begin{aligned} H_{\downarrow\uparrow} = & \Delta_t \sum_{j=1}^{N-1} [d_{j+1\uparrow}^\dagger d_{j\downarrow}^\dagger - d_{j+1\downarrow}^\dagger d_{j\uparrow}^\dagger + h.c.] \\ & + \tilde{\alpha} \sum_{j=1}^{N-1} [d_{j+1\uparrow}^\dagger d_{j\downarrow} - d_{j+1\downarrow}^\dagger d_{j\uparrow} + h.c.] \end{aligned} \quad (24b)$$

Here, σ labels the spin degree of freedom, with $+$ and $-$ denoting the up-spin and down-spin sectors, respectively. The transformed Hamiltonian naturally separates into a down-spin sector H_\downarrow , an up-spin sector H_\uparrow , and a residual inter spin coupling $H_{\downarrow\uparrow}$ containing both induced nonlocal pairing and spin mixing terms. This structure highlights how on site superconducting correlations reshape the effective inter site physics and provides a convenient starting point for exact diagonalization, low-energy modeling, or analytical approximations.

C. Majorana Fermion Representation

We now express the Hamiltonian in Equations (24) in terms of Majorana and bond Fermions. The schematic representation is shown in Fig. 2. To this end, each fermionic operator $d_{j\sigma}$ and its Hermitian conjugate $d_{j\sigma}^\dagger$ is decomposed into two Majorana Fermion operators, $\gamma_{j,1\sigma}$ and $\gamma_{j,2\sigma}$ [1], according to

$$\gamma_{j,1\sigma} = (d_{j\sigma} + d_{j\sigma}^\dagger), \quad \gamma_{j,2\sigma} = i(d_{j\sigma} - d_{j\sigma}^\dagger). \quad (25)$$

These operators are Hermitian, $\gamma_{j,a\sigma}^\dagger = \gamma_{j,a\sigma}$ and satisfy the Majorana anti-commutation relations $\{\gamma_{i,a\sigma}, \gamma_{j,b\sigma'}\} = 2\delta_{ij}\delta_{ab}\delta_{\sigma\sigma'}$.

Using Eq. (25) together with the above anticommutation relations, the Hamiltonians in Eq. (24) can be systematically rewritten entirely in terms of Majorana fermionic operators as

$$H_\sigma = \frac{i}{2} \left[(\tilde{t} + \Delta_\alpha) \sum_{j=1}^{N-1} \gamma_{j+1,2\sigma} \gamma_{j,1\sigma} + (\tilde{t} - \Delta_\alpha) \sum_{j=1}^{N-1} \gamma_{j,2\sigma} \gamma_{j+1,1\sigma} \pm \lambda_\pm \sum_{j=1}^N (\gamma_{j,2\sigma} \gamma_{j,1\sigma} - i) \right] \quad (26a)$$

$$H_{\downarrow\uparrow} = \frac{i(\Delta_t + \tilde{\alpha})}{2} \sum_{j=1}^{N-1} \left[\gamma_{j+1,2\uparrow} \gamma_{j,1\downarrow} - \gamma_{j+1,2\downarrow} \gamma_{j,1\uparrow} \right] + \frac{i(\Delta_t - \tilde{\alpha})}{2} \sum_{j=1}^{N-1} \left[\gamma_{j+1,1\uparrow} \gamma_{j,2\downarrow} - \gamma_{j+1,1\downarrow} \gamma_{j,2\uparrow} \right]. \quad (26b)$$

This representation makes the structure of hopping and pairing processes explicit in the Majorana space and naturally motivates the introduction of new Fermions, which combine neighboring Majorana operators into conventional fermionic degrees of freedom. The Hamiltonian in Eq. (26) explicitly exhibits couplings between different types of Majorana operators on adjacent sites, both within a given spin sector and between opposite spins.

D. Bond Fermion Representation

Although the Hamiltonian in Eq. (26) is not diagonal in the Majorana basis, the specific pattern of these inter spin Majorana pairings suggests a natural reorganization of the degrees of freedom. This observation motivates the definition of a new set of auxiliary fermionic operators, referred to as *bond Fermions* [37], constructed from pairs of Majorana operators

of different types on neighboring sites, as defined below

$$a_{j\sigma} = \begin{cases} \frac{1}{2}(\gamma_{j,1\sigma} - i\gamma_{j+1,2\sigma}), & j = 1, \dots, N-1, \\ \frac{1}{2}(\gamma_{N,1\sigma} - i\gamma_{1,2\sigma}), & j = N. \end{cases} \quad (27)$$

Here, $a_{j\sigma}$ denotes a bond Fermion constructed from two Majorana operators of different types on neighboring sites when $j \neq N$. The operator $a_{N\sigma}$ is defined by pairing the two Majorana operators $\gamma_{1,2\sigma}$ and $\gamma_{N,1\sigma}$, which remain unpaired at the ends of the chain. This fermionic operator corresponds to the zero-energy degree of freedom formed from the Majorana end modes in the topological phase. To diagonalize the Hamiltonian in the bond Fermion basis, we focus on the topological sweet spot of the down spin sector [37], characterized by the conditions

$$\tilde{t} = \Delta_\alpha \Rightarrow t\mu = \alpha\Delta, \quad \lambda_- = 0 \Rightarrow V_z = \sqrt{\mu^2 + \Delta^2}. \quad (28)$$

Under these conditions, the effective Hamiltonian of the down spin (Eq. (26a)) becomes diagonal when expressed in terms of the bond Fermion operators. Consequently, the Hamiltonians in Eq. (26) written in the bond Fermion basis take the form

$$H_\downarrow = \tilde{t} \sum_{j=1}^{N-1} \left(2a_{j\downarrow}^\dagger a_{j\downarrow} - 1 \right) + 0a_{N\downarrow}^\dagger a_{N\downarrow} \quad (29a)$$

$$H_\uparrow = \tilde{t} \sum_{j=1}^{N-1} \left(2a_{j\uparrow}^\dagger a_{j\uparrow} - 1 \right) + 0a_{N\uparrow}^\dagger a_{N\uparrow} + V_z \sum_{j=1}^N (a_{j-1\uparrow}^\dagger a_{j\uparrow}^\dagger + a_{j-1\downarrow}^\dagger a_{j\downarrow}^\dagger + h.c.) + NV_z \quad (29b)$$

$$H_{\downarrow\uparrow} = (\Delta_t + \tilde{\alpha}) \sum_{j=1}^{N-1} (a_{j\uparrow}^\dagger a_{j\downarrow}^\dagger + h.c.) + \frac{(\Delta_t - \tilde{\alpha})}{2} \sum_{j=1}^{N-1} (a_{j+1\uparrow}^\dagger a_{j-1\downarrow}^\dagger - a_{j+1\downarrow}^\dagger a_{j-1\uparrow}^\dagger - a_{j+1\uparrow}^\dagger a_{j-1\downarrow}^\dagger + a_{j+1\downarrow}^\dagger a_{j-1\uparrow}^\dagger + h.c.). \quad (29c)$$

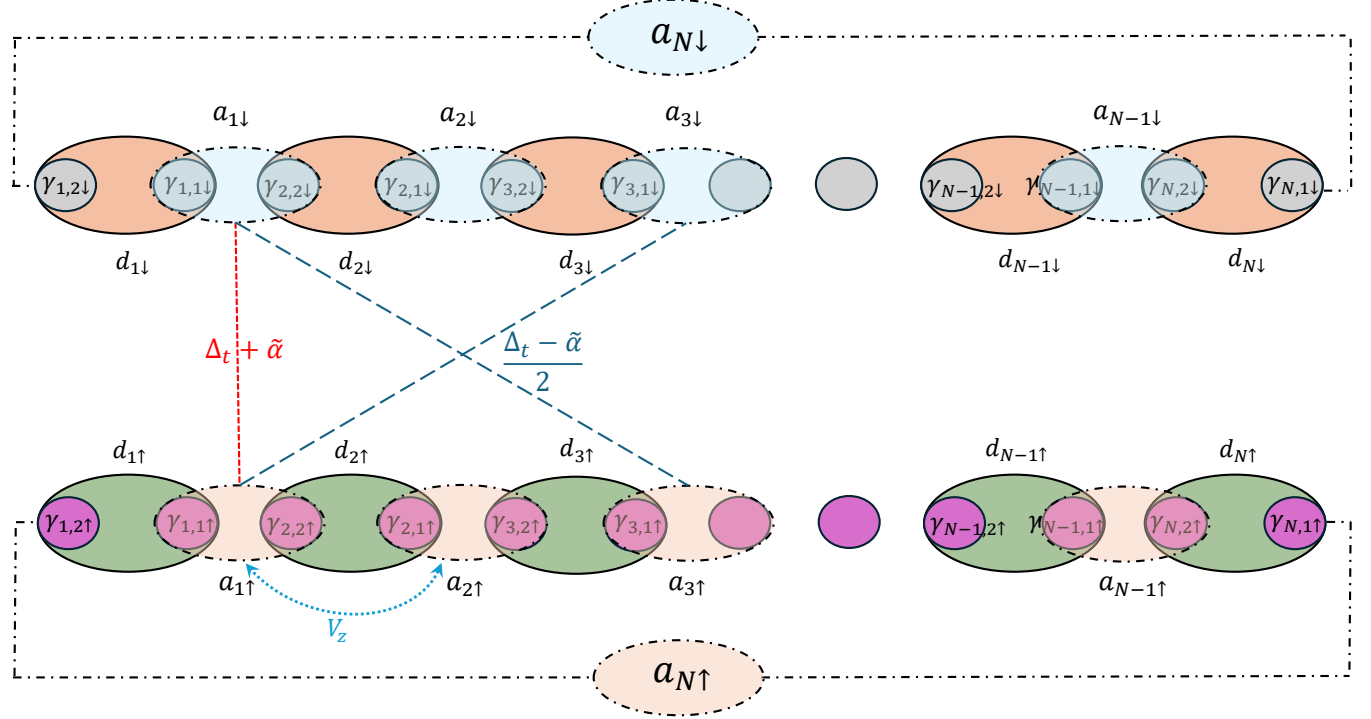


FIG. 2. Schematic of the two coupled Kitaev chains (upper one is for down spin and lower one is for up spin) in the Majorana and bond Fermion representation, with non-zero bond Fermions $a_{j\downarrow}$ and $a_{j\uparrow}$ ($j \neq N$), and the non local zero mode, living on the two ends of the two chains represent as $a_{N\downarrow}$ and $a_{N\uparrow}$. The coupling between the two chains are shown in red and blue dashed lines.

The total Hamiltonian in terms of bond Fermion can be expressed via Eq. (23). Since bond Fermions represent the convenient quasiparticle degrees of freedom of the Kitaev Hamiltonian, their occupation number configurations form a convenient basis for describing the eigenstates of the system. Furthermore, an s -wave Majorana nanowire can be interpreted as two effective p -wave Kitaev chains associated with different spin species. Depending on the system parameters, one of these chains lies in the topological regime while the other is in trivial regime. The two spin chains are coupled through both short and long range superconducting pairing, together with long range Rashba spin orbit coupling.

Motivated by this observation, we employ the bond Fermion occupation basis to perform exact diagonalization of the total Hamiltonian, following the procedure outlined in Eqs. (7)–(10).

IV. RESULTS AND DISCUSSION

Before analyzing the spectrum of the full Hamiltonian, we first examine the energy spectra of the down-spin (H_{\downarrow}) and up-spin (H_{\uparrow}) sectors separately. As shown in Eqs. (29a) and (29b), tuning the system parameters such that the down-spin Hamiltonian satisfies the topological resonance condition inevitably drives the up-spin Hamiltonian away from the topo-

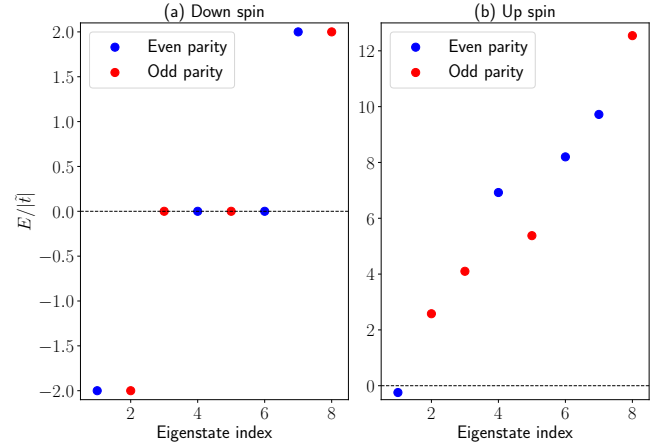


FIG. 3. Energy spectra of the (a) down and (b) up spin chains in the bond Fermion basis, where we enforce the down spin chain to be topological imposing $\tilde{t} = \Delta_{\alpha}$ and $V_z = \sqrt{\mu^2 + \Delta^2}$. The parameters are $N = 3$, $t = \Delta = 1$ and $\alpha = 0.8t$, consequently $\tilde{t} = -0.6247$ and $V_z = 1.2806$. Energy is normalized to $|\tilde{t}|$.

logical regime. The resulting energy spectra for the two spin sectors are shown in Figs. 3(a) and (b).

To illustrate our findings, we fix $N = 3$, $t = \Delta = 1$ and

$\alpha = 0.8t$, otherwise mentioned explicitly. The corresponding values of the chemical potential μ and Zeeman field V_z are determined from Eq. (28), while the remaining parameters are obtained using Eqs. (20) and (22). As noted earlier, the coherent superpositions of the bond Fermion configurations constitute the eigenstates of the system, we perform our calculations on the bond Fermion basis. When the down-spin Hamiltonian is in the topological regime, the system exhibits a doubly degenerate ground state (GS), one in the odd-parity subspace, $|\Psi_{GS}\rangle = |111\rangle_{\downarrow}$, in which all bond Fermions are occupied, and the other in the even-parity subspace, $|\Psi_{GS}\rangle = |110\rangle_{\downarrow}$, which lacks the zero-energy bond fermion $a_N \equiv a_3$. In addition, there are four excited states corresponding to the absence of one non-zero-energy bond fermion, with excitation energy $2|\tilde{t}|$, two in each parity sector. These spectra correctly reproduce the well-known results for the Kitaev chain in the bond-Fermion basis [37]. In contrast, the up-spin Hamiltonian does not exhibit degeneracy between the even and odd parity sectors. The energy eigenstates in each parity sector are instead non degenerate and are given by coherent superpositions of up-spin bond Fermion configurations with different particle numbers, while Fermion parity remains conserved. For instance, the ground state in the even parity sector is a linear combination of $|000\rangle_{\uparrow}$, $|101\rangle_{\uparrow}$, $|110\rangle_{\uparrow}$, and $|011\rangle_{\uparrow}$, whereas the ground state in the odd parity sector is composed of $|100\rangle_{\uparrow}$, $|010\rangle_{\uparrow}$, $|001\rangle_{\uparrow}$, and $|111\rangle_{\uparrow}$. The absence of parity degeneracy and the strong mixing of configurations indicate that the up spin chain resides in a topologically trivial phase. Furthermore, the ground states in the two parity sectors are separated by a large energy gap, and the entire spectrum of the up spin Hamiltonian lies at substantially higher energies compared to that of the down spin chain.

Let us now move to the two coupled Kitaev chain case, for this we are taking our full working Hamiltonian in the bond Fermion basis as $H = H_1 + H_2 + H_{12}$. Again, here we intentionally remove the term $-N(\mu + \sqrt{\mu^2 + \Delta^2})$ as it only shifts the energy scale without affecting the physical interpretations of the energy spectra.

In the absence of inter-chain coupling, the system decomposes into two effectively independent Kitaev chains associated with different spin species. In this limit, the Fermion parity operator $\mathcal{P} = (-1)^N$ commutes with the Hamiltonian and the presence of Majorana zero modes enforces an exact degeneracy between the even and odd parity ground states. Importantly, even at the presence of inter spin coupling, fermion parity remains a good quantum number, and the Hamiltonian block diagonalizes into even and odd parity sectors. This indicates that the inter spin coupling preserves the fundamental particle hole symmetry of the superconducting system. Again, due to the presence of the magnetic field, the Hamiltonian violates time-reversal symmetry. Consequently, the system remains in symmetry class D [47], although the additional approximate chiral symmetry present in the decoupled limit is broken. In a generic interacting superconducting system, one would expect parity dependent energy shifts of order magnitude of coupling.

Figure 4 shows the energy spectra in the (a) even and (b) odd

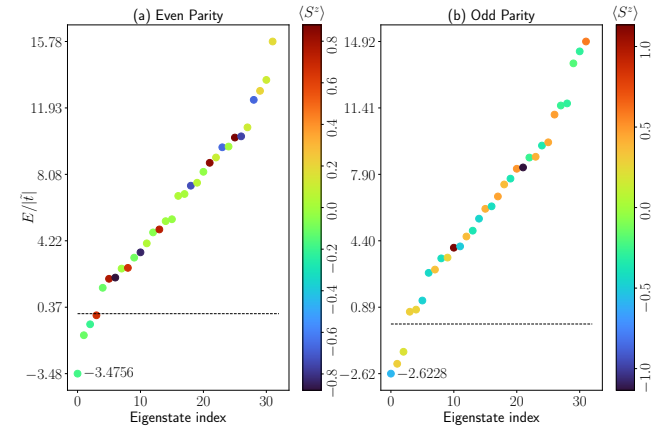


FIG. 4. Energy spectra of the total Hamiltonian and the rest of the parameters are same as Fig. 3. The black dashed lines correspond to zero at both the plots.

Fermion parity sectors for a finite chain of $N = 3$ quantum dots in the presence of inter chain coupling term. In this case, the parity splitting is of order of $|\tilde{t}|$ ($\sim 0.85|\tilde{t}|$), and the lowest even and odd parity states are separated by an energy that exceeds the first excitation scale ($\sim 0.52|\tilde{t}|$). This places the system deep in the strong coupling regime, where the notion of Majorana zero modes is no longer meaningful. Although particle hole symmetry ensures that Fermion parity remains conserved, parity alone does not provide protection against level splitting in this regime, and the system behaves as a topologically trivial superconductor. The spin resolved structure of the eigenstates further clarifies that, for the spinful s -wave Hamiltonian, the low energy excitations are best described as conventional Bogoliubov quasiparticles delocalized across both spin sectors, rather than as spin resolved or spin entangled Majorana modes.

Consequently, for a three-site QD, the system remains in a trivial superconducting phase characterized by strong parity splitting and conventional quasiparticle excitations. This underscores the crucial role of inter spin coupling in controlling the stability of Majorana induced parity degeneracy in realistic spinful s -wave proximity induced SM-SC array of QDs. Overall, the system represents an intermediate crossover between decoupled spin resolved Kitaev chains and a fully hybridized trivial superconductor.

We compute the electronic addition spectral function for the down spin chain in the bond Fermion basis, which quantifies the probability of adding a down spin bond Fermion at bond j to the many body ground state of the system. The local spectral function is defined as

$$A_j(\omega) = \sum_f |\langle \Psi_f | a_{j\downarrow}^\dagger | \Psi_{GS} \rangle|^2 \delta(\omega - (E_f - E_{GS})), \quad (30)$$

where the sum runs over the entire many body eigenstates $|\Psi_f\rangle$, including the ground state and all excited states, with corresponding energies E_f . The delta function enforces energy conservation during the particle addition process. In

numerical calculations, we approximate it by a Lorentzian broadening, $\delta(\omega) \approx \frac{\eta}{\pi[\omega^2 + \eta^2]}$ with the broadening parameter $\eta = 0.05$. Importantly, the spectral function is evaluated in the full Hilbert space, without restricting to a fixed Fermion parity sector. The necessity of this choice becomes clear from the parity structure of the problem. As shown in Eq. (9), any many body wavefunction can be expanded as a linear combination of basis configurations with definite Fermion parity

$$|\Psi\rangle = |\Psi\rangle^{even} + |\Psi\rangle^{odd} = \sum_i D_i^p |i\rangle^{even} + \sum_j C_j^q |j\rangle^{odd} \quad (31)$$

where $|i\rangle^{even}$ and $|j\rangle^{odd}$ denote basis states with even and odd fermion parity, respectively, and D_i^p and C_j^q are the corresponding expansion coefficients. The fermionic creation operator $a_{j\downarrow}^\dagger$ changes the total Fermion number by one and therefore flips the Fermion parity. Consequently, acting with $a_{j\downarrow}^\dagger$ on an even (odd) parity ground state produces a state in the odd (even) parity sector. As a result, only those matrix elements contribute to the spectral function for which the parity of the final state matches the parity obtained after applying the creation operator on the ground state. Taking this parity selection rule into account, the spectral function can be written explicitly as

$$A_j(\omega) = \sum_f |\langle \Psi_f^{odd} | a_{j\downarrow}^\dagger | \Psi_{GS}^{even} \rangle|^2 \delta(\omega - (E_f - E_{GS})) + \sum_f |\langle \Psi_f^{even} | a_{j\downarrow}^\dagger | \Psi_{GS}^{odd} \rangle|^2 \delta(\omega - (E_f - E_{GS})). \quad (32)$$

This formulation makes explicit that the electronic addition spectral function necessarily involves both Fermion parity sectors, justifying our use of the full Hilbert space in the numerical evaluation.

The spectral function of the down spin bond fermion provides direct microscopic insight into the role of coupling between the two spin chains and allows us to connect these effects to experimentally measurable tunneling signals, such as the differential conductance dI/dV_{SD} , where V_{SD} denotes the source-drain voltage. In tunneling experiments, the local differential conductance is proportional to the local density of states, which in turn is directly related to the site resolved spectral function evaluated at the tunneling position. This site resolution is crucial, since Majorana zero modes are spatially localized near the ends of the chain and would be obscured in spatially bulk spectral quantities [48].

In particular, the presence of a zero energy peak in the spectral function signals a low energy quasiparticle excitation localized at the end of the chain. In our case, this feature is associated with the zero energy bond fermion $a_{N\downarrow}$, which plays the role of a Majorana zero mode. Consequently, the corresponding spectral weight is sharply concentrated around zero frequency, giving rise to a pronounced zero bias peak in the tunneling conductance. The evolution and robustness of this

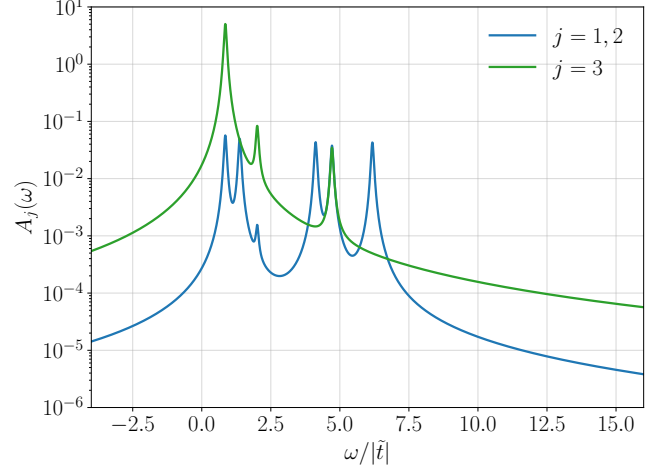


FIG. 5. Site resolved spectral functions $A_j(\omega)$ of the down spin bond Fermions for the chain of $N = 3$ quantum dots, evaluated at the chain end and in the bulk. The spectral function is computed with respect to the many-body ground state using exact diagonalization and includes a finite broadening η . Low-energy spectral weight is strongly localized at the chain ends, while bulk contributions remain suppressed, indicating boundary localized Majorana like excitations whose hybridization.

zero frequency feature therefore provide a direct probe of Majorana physics and of the influence of inter chain coupling on the low energy excitation spectrum.

Figure 5 shows the bond resolved spectral function $A_j(\omega)$ of the down spin chain for an $N = 3$ quantum dot system, evaluated at bonds $j = 1, 2, 3$. The spectra are plotted as a function of frequency $(\omega/|\tilde{t}|)$, with a logarithmic scale used on the spectral-function axis to highlight the large dynamic range of spectral weights. A striking feature of the figure is the pronounced spatial inhomogeneity of the low-energy spectral weight. The dominant low-energy resonance appears exclusively at the terminal bond $j = 3$, while the interior bonds $j = 1$ and $j = 2$ exhibit strongly suppressed spectral weight in the low-frequency window and are instead dominated by higher-energy excitations.

This pronounced bond selectivity indicates that the lowest-lying excitation couples predominantly to an edge localized degree of freedom rather than to bulk like quasiparticles. Although the dominant peak at $j = 3$ is shifted away from exactly zero frequency, reflecting finite-size effects and inter-chain hybridization, it remains clearly separated from the bulk excitation continuum. In contrast, the interior bonds show only weak low-energy response, with spectral weight redistributed toward higher energies, signaling enhanced mixing between edge and bulk sectors. The low-energy spectral weight at the terminal bond exceeds that of the interior bonds by roughly two orders of magnitude, demonstrating that the edge localized character of the low-energy mode is robust against inter spin coupling at this system size.

The persistence of a finite energy but strongly edge enhanced

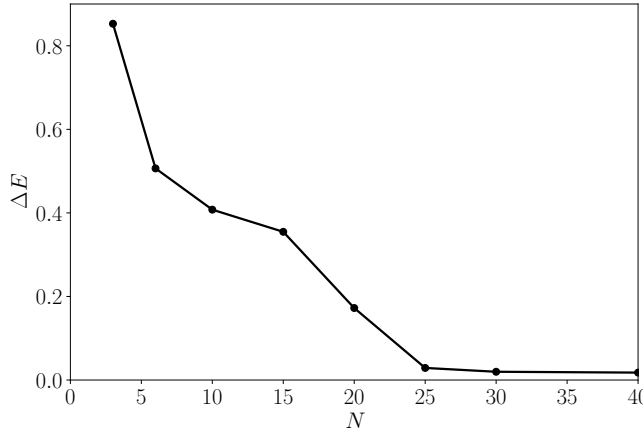


FIG. 6. Finite size scaling of the even odd parity splitting $\Delta E = |E_0^{\text{even}} - E_0^{\text{odd}}|$ as a function of number of QDs in the chain. ED results are shown for short QD systems ($N = 3$ and 6), while DMRG results extend the analysis to longer chains up to $N = 40$.

low-energy resonance is consistent with a hybridized Majorana like mode in a finite system. Such a mode is expected to evolve continuously toward a true zero energy Majorana bound state as the chain length increases, provided the system remains in the topological regime, with the residual splitting vanishing exponentially with system size.

More generally, upon approaching a topological phase boundary one expects the bulk gap to soften and the Majorana localization length to diverge, leading to a qualitative redistribution of low-energy spectral weight from the edge into the bulk and the eventual disappearance of a sharply localized edge resonance. The absence of such a qualitative restructuring in the present spectra suggests that the system remains on the topological side of the phase transition for the parameters considered. The bond resolved spectral function thus provides a dynamical probe of bulk edge correspondence in this minimal $N = 3$ QD chain. The observed edge dominated low-energy response can be characteristic of so-called “poor man’s Majorana” modes, whose topological protection is limited by finite size splitting and inter spin hybridization.

Figure 6 shows the Fermion parity splitting $\Delta E = |E_0^{\text{even}} - E_0^{\text{odd}}|$, where E_0^{even} and E_0^{odd} denote the ground-state energies in the even and odd parity sectors, respectively. The results are obtained from ED for $N = 3$ and 6 , and are complemented by density-matrix renormalization group (DMRG) calculations extending the system size up to $N = 40$, implemented using the ITensor library [49]. The parity splitting of the ground states ΔE decreases monotonically with system size, signaling a nonlocal finite-size splitting mechanism associated with Majorana hybridization. While ED at $N \leq 6$ can therefore give the impression of a crossover to a strongly hybridized regime, since ΔE remains sizable within the limited ED window. The DMRG results demonstrate that this is predominantly a finite-size effect, upon increasing N well beyond the ED accessible sizes, ΔE continues to decrease.

Again, let us return to Eqs. (29), which form the basis of our analysis. Our primary objective is to realize Majorana zero modes, or equivalently in our formulation, zero-energy bond Fermions.

From the structure of the effective Hamiltonian, an important asymmetry between the two spin sectors becomes apparent. The zero-energy bond Fermion associated with the up-spin Hamiltonian (see Eq. (29b)) is coupled to bulk bond Fermions of the same spin through the Zeeman field, and additionally hybridizes with the down-spin sector via inter spin coupling terms. As a result, this zero-energy mode is strongly entangled with the bulk degrees of freedom and cannot be straightforwardly isolated.

In contrast, the zero-energy bond Fermion of the down-spin Hamiltonian (see Eq. (29a)) does not couple to bulk modes within the same spin sector. Its only coupling arises through inter spin terms connecting it to bulk bond Fermions of the up-spin chain. Consequently, if one could devise a protocol to suppress this inter spin hybridization, the down-spin zero-energy bond fermion would become effectively decoupled from the rest of the spectrum. This would yield a robust Majorana mode that is insensitive to the coupling between the two spin sectors.

Such a decoupling occurs only when the effective parameters satisfy the conditions

$$\tilde{\alpha} = \Delta_t \quad \text{and} \quad \tilde{t} = \Delta_\alpha, \quad (33)$$

which simultaneously imply

$$t\Delta = -\alpha\mu, \quad (34a)$$

$$t\mu = \alpha\Delta. \quad (34b)$$

To analyze the feasibility of these constraints, we first note that, in an experimental setting, the chemical potential μ must remain real in a Hermitian Hamiltonian. Similarly, the Rashba SOC is an intrinsic property of the material and is real in equilibrium. Consequently, only selected parameters may acquire complex phases, and we parameterize them as

$$t = |t|e^{i\phi}, \quad \Delta = |\Delta|e^{i\theta}, \quad \alpha = |\alpha|, \quad \mu = |\mu|. \quad (35)$$

Solving these relations yields $\phi = \theta = \pi/2 \pmod{2\pi}$. Therefore, a consistent solution exists if the relative phases between the superconducting pairing and the chemical potential, as well as between the hopping and Rashba spin orbit coupling, differ by a quarter turn. Equivalently,

$$\frac{\Delta}{\mu} = e^{i\theta} = e^{i\pi/2}, \quad \frac{t}{\alpha} = e^{i\phi} = e^{i\pi/2}. \quad (36)$$

From an experimental perspective, it is important to clarify the physical meaning of these phases. Eq. (36) indicates that non-trivial phases may reside only in the hopping amplitude t and in the superconducting pairing Δ . Both quantities can, in principle, be complex, with their Hermitian conjugates appearing

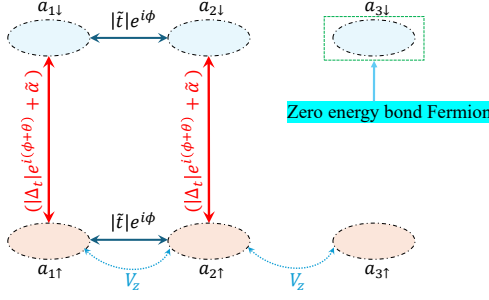


FIG. 7. Pairing non-zero energy bond Fermions with neighboring sites leaves a single zero energy bond Fermion localized at the end of the down spin chain. The schematic is shown for a three site quantum dot system. However, the same construction yields a zero energy bond Fermion independent of system size and inter spin coupling

explicitly in the Hamiltonian. The phase of the superconducting pairing Δ is intrinsic and can be controlled via superconducting phase bias. In contrast, a complex phase associated with the hopping amplitude t is absent in static equilibrium systems and can generally be eliminated by a gauge transformation. This situation is illustrated in Fig. 7, which shows an isolated zero energy bond Fermion localized at the end of the down spin chain. However, such phases may emerge effectively in the presence of gauge fields, orbital magnetic flux, or under Floquet (time-periodic) driving. In such cases, the analysis must begin with hopping and pairing terms carrying a relative phase of $\pi/2$, ensuring that the Hamiltonian remains Hermitian. Under this choice, the resulting inter chain coupling terms become real, leading to the consistent effective description discussed above. A complete assessment of the physical realization and robustness of these phase conditions therefore requires an analysis beyond the static equilibrium framework.

V. CONCLUSIONS

We studied a spinful one-dimensional semiconductor-superconductor model with Rashba spin-orbit coupling, Zeeman splitting, and proximity-induced s -wave pairing, motivated by quantum-dot chains in hybrid nanowires. Using a local BdG transformation we rewrote the Hamiltonian as two coupled Kitaev-like sectors associated with opposite spins, and expressed the resulting problem in Majorana and bond-fermion variables to make the parity structure and low-energy degrees of freedom transparent.

With fermion-parity-resolved exact diagonalization we showed how near-degeneracy between the lowest even- and odd-parity states arises only when one effective sector is tuned into the topological regime, while the other remains trivial. Bond-resolved addition spectral functions exhibit strongly edge-enhanced low-energy spectral weight, whereas inter-spin couplings lift the parity degeneracy and redistribute spectral weight in finite systems. We also identified parameter conditions in the bond-fermion description that suppress the hybridization of the down-spin end mode, providing a concrete route toward more robust zero-energy boundary states within this spinful s -wave framework.

ACKNOWLEDGMENTS

This work was supported by the Quantum Sensors Challenge Program QSP-078, High Throughput Networks HTSN-341, and Applied Quantum Computing AQC-004 Challenge Programs at the National Research Council of Canada, NSERC Discovery Grant No. RGPIN- 2019-05714, NSERC PQS2D Alliance Quantum Grant No. ALLRP/578466-2022. This work was partly enabled by support provided by the Digital Research Alliance of Canada [50].

[1] A. Y. Kitaev, *Physics-Uspekhi* **44**, 131 (2001).

[2] J. Alicea, *Rep. Prog. Phys.* **75**, 076501 (2012).

[3] C. W. J. Beenakker, *Annu. Rev. Condens. Matter Phys.* **4**, 113 (2013).

[4] E. Prada, P. S.-Jose, M. W. A. de Moor, A. Geresdi, E. J. H. Lee, J. Klinovaja, D. Loss, J. Nygård, R. Aguado, and L. P. Kouwenhoven, *Nat. Rev. Phys.* **2**, 575 (2020).

[5] C. Nayak, S. H. Simon, A. Stern, M. Freedman, and S. Das Sarma, *Rev. Mod. Phys.* **80**, 1083 (2008).

[6] J. Alicea, Y. Oreg, G. Refael, F. von Oppen, and M. P. A. Fisher, *Nature Physics* **7**, 412 (2011).

[7] D. Aasen, M. Hell, R. V. Mishmash, A. Higginbotham, J. Danon, M. Leijnse, T. S. Jespersen, J. A. Folk, C. M. Marcus, K. Flensberg, and J. Alicea, *Phys. Rev. X* **6**, 031016 (2016).

[8] J. Bardeen, L. N. Cooper, and J. R. Schrieffer, *Phys. Rev. B* **108**, 1175 (1957).

[9] M. Tinkham, *Introduction to Superconductivity*, 2nd ed. (McGraw-Hill, New York, 1996).

[10] P. G. de Gennes, *Superconductivity of Metals and Alloys* (Benjamin, New York, 1966).

[11] R. M. Lutchyn, J. D. Sau, and S. Das Sarma, *Phys. Rev. Lett.* **105**, 077001 (2010).

[12] Y. Oreg, G. Refael, and F. von Oppen, *Phys. Rev. Lett.* **105**, 077001 (2010).

[13] E. M. Stoudenmire, J. Alicea, O. A. Starykh, and M. P. A. Fisher, *Phys. Rev. B* **84**, 014503 (2011).

[14] J. B.-Chouinard, M. Korkusinski, A. Bogan, P. Barrios, P. Waldron, K. Watanabe, T. Taniguchi, J. Pawłowski, D. Miravet, P. Hawrylak, A. L.-Mayer, and L. Gaudreau, *Sci. Adv.* **11**, 4696 (2025).

[15] Z. Wang, P. Yu, H. Zhang, D. Xu, H. Zhang, C.-X. Liu, and S. M. Frolov, *Phys. Rev. Lett.* **129**, 167702 (2022).

[16] J. Pawłowski, D. Miravet, M. Bieniek, M. Korkusinski, J. Boddison-Chouinard, L. Gaudreau, A. Luican-Mayer, and P. Hawrylak, *Phys. Rev. B* **110**, 125147 (2024).

[17] H. Pan and S. Das Sarma, *Phys. Rev. Res.* **2**, 013377 (2020).

[18] S. Das Sarma and H. Pan, *Phys. Rev. B* **103**, 195158 (2021).

[19] J. Chen, P. Yu, J. Stenger, M. Hocevar, D. Car, S. R. Plissard, E. P. A. M. Bakkers, S. Wang, C. Zhang, and S. M. Frolov, *Sci. Adv.* **3**, e1701476 (2017).

[20] Z. Su, A. B. Tacla, M. Hocevar, D. Car, S. R. Plissard, E. P. A. M. Bakkers, A. J. Daley, D. Pekker, and S. M. Frolov, *Nat. Commun.* **8**, 585 (2017).

[21] A. Ptak, A. Cichy, and T. Domański, *Journal of Physics: Condensed Matter* **30**, 355602 (2018).

[22] T. Dvir, G. Wang, N. van Loo, C.-X. Liu, G. P. Mazur, A. Bordin, S. L. D. ten Haaf, J.-Y. Wang, D. van Driel, F. Zatelli, X. Li, F. K. Malinowski, S. Gazibegovic, G. Badawy, E. P. A. M. Bakkers, M. Wimmer, and L. P. Kouwenhoven, *Nature* **614**, 445 (2023).

[23] A. Bordin, C.-X. Liu, T. Dvir, F. Zatelli, S. L. D. ten Haaf, D. van Driel, G. Wang, N. van Loo, Y. Zhang, J. C. Wolff, T. Van Caekenberghe, S. Gazibegovic, E. P. A. M. Bakkers, M. Wimmer, L. P. Kouwenhoven, and G. P. Mazur, *Nat. Nanotechnol.* **20**, 726 (2025).

[24] C.-X. Liu, A. M. Bozkurt, F. Zatelli, S. L. D. ten Haaf, T. Dvir, and M. Wimmer, *Commun. Phys.* **7**, 235 (2024).

[25] W. Samuelson, V. Svensson, and M. Leijnse, *Phys. Rev. B* **109**, 035415 (2024).

[26] M. Leijnse and K. Flensberg, *Semicond. Sci. Technol.* **27**, 124003 (2012).

[27] S. L. D. ten Haaf, Q. Wang, A. M. Bozkurt, C.-X. Liu, I. Kulesh, P. Kim, D. Xiao, C. Thomas, M. J. Manfra, T. Dvir, M. Wimmer, and S. Goswami, *Nature* **630**, 329 (2024).

[28] S. L. D. ten Haaf, Y. Zhang, Q. Wang, A. Bordin, C.-X. Liu, I. Kulesh, V. P. M. Sietses, C. G. Prosko, D. Xiao, C. Thomas, M. J. Manfra, M. Wimmer, and S. Goswami, *Nature* **641**, 890 (2025).

[29] J. Benestad, A. Tsintzis, R. Seoane Souto, M. Leijnse, E. van Nieuwenburg, and J. Danon, *Phys. Rev. B* **110**, 075402 (2024).

[30] M. Krawczyk and J. Pawłowski, *arXiv:2601.02149* (2026).

[31] M. Cygorek, M. Korkusinski, and P. Hawrylak, *Phys. Rev. B* **101**, 075307 (2020).

[32] J. Manalo, M. Cygorek, A. Altintas, and P. Hawrylak, *Phys. Rev. B* **104**, 125402 (2021).

[33] D. Dalacu, K. Mnaymneh, J. Lapointe, X. Wu, P. J. Poole, G. Bulgarini, V. Zwiller, and M. E. Reimer, *Nano Lett.* **12**, 5919 (2012).

[34] J. Phoenix, M. Korkusinski, D. Dalacu, P. J. Poole, P. Zawadzki, S. Studenikin, and L. Gaudreau, *Sci. Rep.* **12**, 5164 (2022).

[35] J. Manalo, D. Miravet, and P. Hawrylak, *Phys. Rev. B* **109**, 085112 (2024).

[36] M. Mohseni, I. Cunha, D. Miravet, A. Wania Rodrigues, H. Al-lami, I. Assi, M. Korkusinski, and P. Hawrylak, *physica status solidi (b)* **262**, 2400552 (2025).

[37] M. Mohseni, H. Allami, D. Miravet, D. J. Gayowsky, M. Korkusinski, and P. Hawrylak, *Nanomaterials* **13**, 2293 (2023).

[38] M. J. J. Mangnus, J. W. de Wit, S. J. W. Vonk, J. J. Geuchies, W. Albrecht, S. Bals, A. J. Houtepen, and F. T. Rabouw, *ACS Photonics* **10**, 2688 (2023).

[39] P. Laferriere, E. Yeung, M. Korkusinski, P. J. Poole, R. L. Williams, D. Dalacu, J. Manalo, M. Cygorek, A. Altintas, and P. Hawrylak, *Appl. Phys. Lett.* **118**, 161107 (2021).

[40] Y. Al-Douri, M. M. Khan, and J. R. Jennings, *J. Mater. Sci.: Mater. Electron.* **34**, 993 (2023).

[41] H. Pan and S. Das Sarma, *Phys. Rev. B* **107**, 035440 (2023).

[42] A. Arora, A. Kejriwal, and B. Muralidharan, *New Journal of Physics* **26**, 023038 (2024).

[43] E. F. Talantsev, K. Iida, T. Ohmura, T. Matsumoto, W. P. Crump, N. M. Strickland, S. C. Wimbush, and H. Ikuta, *Scientific Reports* **9**, 14245 (2019).

[44] W. S. Wang, C. C. Zhang, F. C. Zhang, and Q. H. Wang, *Phys. Rev. Lett.* **122**, 027002 (2019).

[45] N. F. Yuan, K. F. Mak, and K. Law, *Phys. Rev. Lett.* **113**, 097001 (2014).

[46] F. Hardy and A. D. Huxley, *Phys. Rev. Lett.* **94**, 247006 (2005).

[47] A. P. Schnyder, S. Ryu, A. Furusaki, and A. W. W. Ludwig, *Phys. Rev. B* **78**, 195125 (2008).

[48] R. Thomale, S. Rachel, and P. Schmitteckert, *Phys. Rev. B* **88**, 161103(R) (2013).

[49] M. Fishman, S. R. White, and E. M. Stoudenmire, *SciPost Phys. Codebases* **4** (2022).

[50] Digital Research Alliance of Canada, Digital Research Alliance of Canada, <https://alliancecan.ca> (2025), accessed: 2025-07-26.